http://dx.doi.org/10.21611/qirt.1992.040

Some new ideas in dynamic thermal tomography

by V. VAVILOV(*), P.G. BISON(**), C. BRESSAN(**), E. GRINZATO(**) and S. MARINETTI(**)

(*) Tomsk Polytechnic Institute, Tomsk, Russia.

(**) Consiglio Nazionale delle Ricerche, Istituto per la Tecnica del Freddo (ITEF), Padova, Italy.

Abstract

Dynamic Thermal Tomography (DTT) is a new area of Thermal Non Destructive Techniques (TNDT), very attractive for *in field* detection of defects inside materials. It is based on the energetic excitation of solids, resulting in the dynamic distribution of the temperature field on their surface. Defects, inside the solid, change the evolution and the distribution of the surface temperature field. Solving the inverse thermal problem, which involves the processing of surface temperature field, one gets information on the inner structure of solids.

Tests has been performed on two specimens compound of 5 layers, with thickness 1.8 mm each. Air holes in internal layers, performed in different shapes and arrangements, simulate defects. Another defect was simulated by a lack of glue.

The results for the surface temperature in correspondence of defects show a dependence with time close to that of the simulated curves. Synthesized images of different inner layers of the material show the presence of defects whose position and depth are in good accordance with those of the real one, as it has been verified after destroying the specimens at the end of the experiment.

Nomenclature

a	diffusivity	$m^2.s^{-1}$
A_n	noise contrast	°C/°C
d	thickness of defect	mm
ΔT	temperature difference between defect and non-defect zones on specimen's surface	°C
$\Delta T_m = \Delta T\ (\tau_m)$		°C
l	depth of defect	mm
λ	thermal conductivity	$W.m^{-1}.K^{-1}$
MED	averaged value of temperature signal in predetermined area	°C
Q	specific heat flux	$W.m^{-2}$
σ	standard deviation of temperature signal	°C
τ_m	time of maximum ΔT value	s

1. Introduction

Dynamic thermal tomography (DTT) which seemed to be included into the thermal NDT agenda for the last two years is still remaining as intuitive or if to say more correctly phenomenological technique [1-4]. Its simple physical idea somehow contradicts to the basic mathematical description which is hardly to be done analytically, requiring to study 2D or 3D models [1-5]. Up to now we could make the following statements concerning the main DTT principles and results:

- DTT involves one-side active NDT procedure based on the storing of multiple IR images;

- time-dependant surface signal represents the sum of temperature responses of some internal areas starting from the tested surface; the relative contribution of internal layers is changing in time too; the more is time delay after heating the deeper layers could be probed;

- DTT being the modification of the standard thermal NDT experiences strong sensitivity decrease with deeper layers to be involved;

- DTT is mostly effective to detect the *look-like-discontinuity* defects being rather insensitive toward the variations of the internal thermal properties;

- number of experimentally resolved layers was reported of about 8 [2] although theoretical value up to 40 layers was predicted [5];

- the first practical results of DTT have been found in the investigation of fatigue damages in carbon fibre epoxy plastics [3-5].

http://dx.doi.org/10.21611/qirt.1992.040

We believe that DTT technique is now surviving the initial period when basic terminology and processing algorithms are establishing. We shall concentrate our present investigation on some new ideas (application of pattern recognition approach and cross-sectional timegrams) which could lead to the higher DTT resolution.

2. Equipment and procedure

Recording of dynamic temperature field was performed with IR imager Thermovision-782, Agema. A digital processing system developed in the Istituto per la Tecnica del Freddo, Padova, Italy, was used to grab the sequence of IR images each 0.3-3.0 s. A number of images in a set varied from 48 to 128 (ram or high-speed hard disk memory). The frame format was chosen as 8-bit, 256x256 pixels picture. The grabbing process was performed through the special unit linked to MacIntosh computer [7] backed with standard and home-made (TIPS [8], TOMOS) software. Before processing the set of grabbed images was compressed that meant the simultaneous low-frequency spatial filtering too.

Two standard specimens of plastic with size 110x110 and140x140 mm consisted of 5 layers with thickness 1.8 mm each. Air holes in internal layers performed in shape of cross, triangle and square, served as artificial defects so the defects' thickness was 1.8 mm and defects' depth varied from 1.8 to 5.4 mm. Another defect was simulated by a lack of glue at the depth 1.8 mm. Scheme of specimens is
260 shown in *figure 1.* The specimens' surface was covered with *Graphite-33* spray providing the emissivity of 0.98. A strip-shaped 2000 W quartz halogen lamp with reflector heated the specimens up to 25 °C above ambient for 10 s. The technically determined time delay between end of heating and the first successfully grabbed image was about 1.5 s in one-side procedure. Two-side procedure was used too for the measurement of diffusivity by Parker's method.

3. *A priori* estimates

Theoretical estimates of parameters involved have been done before to choose the suitable DTT algorithm using the *Test-2D* program (Tomsk Polytechnic Institute) composed for solution of 2D cylindrical DTT problem [5]. Calculation of three locations of defects allowed to obtain two main functions necessary for DTT: 1) time evolution of the temperature signal ΔT upon the defect; 2) dependence of some specific heat transfer times (like time τ_m when maximum of ΔT is reached). These functions shown in *figure 2* allowed to choose the appropriate time range of heating-cooling process and grabbing time gap. Thermal properties values have been obtained experimentally by using the Parker's flash method (λ=0.325 $W.m^{-1}.K^{-1}$; a=2.68 $10^{-7}m^2.s^{-1}$. The heat flux density effectively absorbed by a specimen was measured with *Appley* solar radiation radiometer at the level of 7550 $W.m^2$.

Thermal tomograms synthesized earlier revealed the high noise level if not being processed with threshold technique [5,6]. In our experiments we thoroughly studied the statistical behaviour of surface noise in space and time. The *temperature contrast* terminology was accepted for the noise description [4]. Noise contrast was determined as $A_n=\sigma/MED$, where σ is the standard deviation and *MED* the averaged value of noise in the pre-determined area. It was found that for chosen specimens the A_n value varied in time from 1.2 % to 3.2 % during 120 s of cooling. The best results have been obtained with an averaged area 8x8 mm on the specimen's surface. Variations of noise over the whole surface were in a range of 1.2-2.1 % (if operator specified the non-defect area to be large as much as possible the A_n value was about 4 %). Additionally the statistic parameters of noise have been found for a non-defect plate consisting of one plastic layer. Noise contrast for two non-defect specimens (without and with black paint) was in a range 1.0-1.2 % in the area 8x8 mm. If the whole area of specimen (110x110 mm) was specified the noise level has been increasing up to 4.4-4.9 % probably because of non-uniform heating-cooling. These results are in good agreement with previously reported data [6] so in the DTT procedure the noise amplitude was chosen at the level of 2 or 3 standard deviations i.e. threshold value was 2.5-4 % in the most interesting time interval. It is worth saying that spatial filtration decreased noise down to zero level if the averaged area was placed in the centre of specimen (between defects).

4. DTT algorithm

Generally the used DTT algorithm corresponded to the one proposed in [1]. Nevertheless in order to avoid too *noisy* presentation of tomograms we replaced the time filtering with function

http://dx.doi.org/10.21611/qirt.1992.040

approximation. Really the experimental time evolution of ΔT signal (see *figure 2*) shows clearly the problems with finding the specific heat transfer time $\tau_{m.d.}$, $\tau_{+0.72}$, τ_m, $\tau_{-0.72}$ which were proposed in [5] to specify the evolution function for each pixel. Assuming that each pixel history is created by difference between two look-like-exponent function we performed the exponential approximation.

Another new step in our considerations concerned the *cross-sectional timegram* which is obtained by slicing the *data parallelepiped* formed by two surface coordinates and time (in our case the parallelepiped size was 256x256x48 pixels). Traditional thermograms are obtaining by slicing the data parallelepiped by the planes perpendicular to time-axis as well as ordinary timegrams represent the distribution of one accepted specific time over the surface. Cross-sectional timegrams have to be synthesized by slicing the parallelepiped with planes perpendicular to *X*- or *Y*-axis producing the time evolution of temperature or temperature defect signal along the surface line (or any curve in general).

5. Experimental results

Experimental ΔT curves for two defects at the depth l = 1.8 and 3.6 mm are shown in *figure 2a*. Comparing with theory the error in determining τ_m was less than 5 % but for temperature signal it reached 70 % probably due to not-accurate measurement of Q value. The function τ_m vs defect depth l which could be viewed as the calibration curve for tomography is presented in *figure 2b* for an air defect with thickness 1.8 mm.

The examples of initial images for both specimens are presented in *figure 3* in grey scale mode (non-filtered in *figure 3a* and after filtration in *figure 3b*) and 3D presentation(*figures 3c,d*).

Two synthesized ΔT_m and τ_m images are given in *figure 4*. Their comparison shows that the ΔT_m image could be used for tomography by sorting the amplitude out only in a case of defects with one thickness (*figure 4a*). Defects 1,2,3 produce the decreasing signal but the defect 4 located at the same depth as 1 produces the signal at the level of deepest defect 3. On the contrary the timegram of *figure 4b* shows clearly the highest level of τ_m for defect 3 although in this case too the defect thickness d influences the τ_m value (in details see [6]).

The normalized (sliced) thermal tomograms for eight layers are presented in *figure 5* for a time delay interval of 6 s (*figures 5e,f*) and 12 s (*figures 5g,h*). The coordinates of particular layer (in terms of air defect with thickness 1.8 mm) could be easily found from the gauging curve of *figure 2b*. For instance, the tomogram of *figure 5e* corresponds to a delay time range 24-30 s and to the depth layer 3.3-3.9 mm (*figure 1*) containing the defect 2 at the depth 3.6 mm. Tomograms of *figure 5* show that the results for the shallow layers (*figures 5a,b*) are the most sensitive for any structural non-uniformity, influence of which is decreasing with depth. It is worth saying that the thin defect 4 is seen best of all in the first tomogram (*figure 5a*) because it creates a smaller delay time than defect 1 at almost the same depth. Generally all four defects are seen at the particular tomograms although the deepest defect 3 shows the abnormal area much smaller than its real size (*figure 5h*). The results above resemble very much the data for another material published earlier [6]. The main disadvantage of timegrams and tomograms like these is the presence of artefacts surrounding the defect area (it is seen best of all in *figure 5c*) because of different delay times for central and peripheral points of the defect area. We explain this by 3D character of heat transfer.

Two tomograms for specimen 2 are presented in *figure 6* in normal and sliced mode for the delay time range 7-35 s showing defects 5,6 and not the defects 7,8. So far our technique failed to separate the defects 5 and 7.

Cross-sectional timegram of the specimen 1 obtained for the vertical line crossing the defects 1 and 2 is shown in *figure 7* using the slicing technique together with profiles which in fact repeat the functions in *figure 2a*. The artefact around defect 1 in *figure 7b* is seen again.

Finally the specimens have been destroyed after the experiments in order to compare the real situation in bonded areas with DTT data. The scheme of artificial and real defects is shown in *figure 8* for two bonded areas superimposed on each other. It could be seen that tomograms give more details relating some defective areas which are not seen in the ordinary thermograms. The depth of detected defects in our experiments was about 5.4 mm for holes and 3.6 mm for a lack of glue.

http://dx.doi.org/10.21611/qirt.1992.040

6. Conclusion

Getting some experience in synthesis of thermal tomograms we believe that the main problems of the practical application of this technique is the great deal of information which is multiplied by a variety of image processing algorithm. It requires very accurate technique to compare the synthesized and real pictures of bonded areas. Another problem is the presence of artefacts which could lead to wrong presentation of in-depth defects' penetration.

REFERENCES

[1] VAVILOV (V.). - *Dynamic thermal tomography: Perspective field of thermal NDT.* Proc. SPIE, vol. 1313, Thermosense-XII,1990,p. 307.

[2] VAVILOV (V.), AHMED (T.), JIN (J.), THOMAS (R.L.) and FAVRO (L.D.). - *Experimental thermal tomography of solids by using the flash one-side heating.* Sov. J. NDT, 1990, N°.12, p. 60.

[3] VAVILOV (V.), DEGIOVANNI (A.), HOULBERT (A.S.), MAILLET (D.) and DIDIERJEAN (S.). - *Thermal testing and tomography of carbon epoxy plastics.* Sov. J. NDT, 1991 (to be published).

[4] FAVRO (L.D.), AHMED (T.), JIN (J.), THOMAS (R.L.) and KUO (P.K.). - *Infrared thermal wave studies of coatings and composites.* Proc. SPIE, vol. 1467, Thermosense-XIII, 1991, p. 290.

262 [5] VAVILOV (V.), MALDAGUE (X.), PICARD (J.), THOMAS (R.L.) and FAVRO (L.D.). - *Dynamic thermal tomography: new NDE technique to reconstruct inner solids structure using multiple IR image processing.* Rev. of Progress in Quantit. NDE, Bowdoin College, Maine, USA, 1991, 31 July (to be published).

[6] VAVILOV (V.). - *Infrared techniques for materials analysis and non-destructive testing*: Infrared Technique for NDT, ed. by X. Maldague, Gordon & Breach Science Publisher, N.Y., 1991 (to be published).

[7] BISON (P.G.), BRAGGIOTI (A.), CORTELAZZO (G.M.), GRINZATO (E.), MAZZOLDI (A.) and MIAN (G.A.). - *Open architecture for multispectral computer vision applied to both visual and infrared bands.* Proc. SPIE, vol. 1349, San Diego (USA), 8-13 July,1990.

[8] GRINZATO (E.). - *Dedicated image processing for thermographic NDT.* Infrared Technique for NDT, ed. by X. Maldague, Gordon & Breach Science Publisher, N.Y., 1991 (to be published).

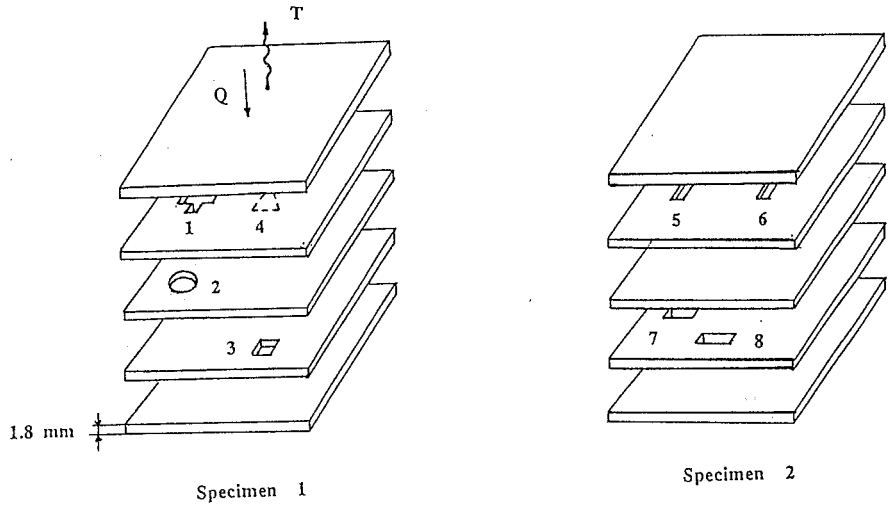

Fig. 1. - Scheme of defects in plastic specimens (defects 1,2,3,5,6,7,8-air holes; defect 4-lack of glue)

http://dx.doi.org/10.21611/qirt.1992.040

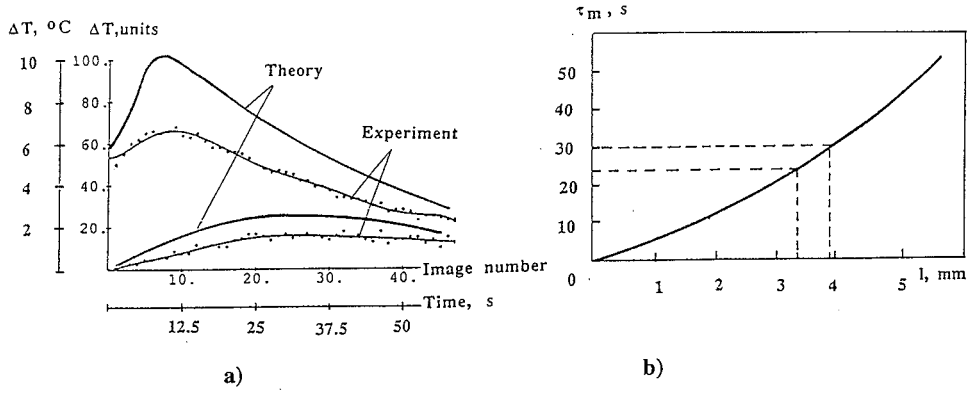

Fig. 2. - Temporal functions important in DTT: a) ΔT vs τ (specimen 1, defects 1,2); b) τ_m vs l (defects 1,2,3)

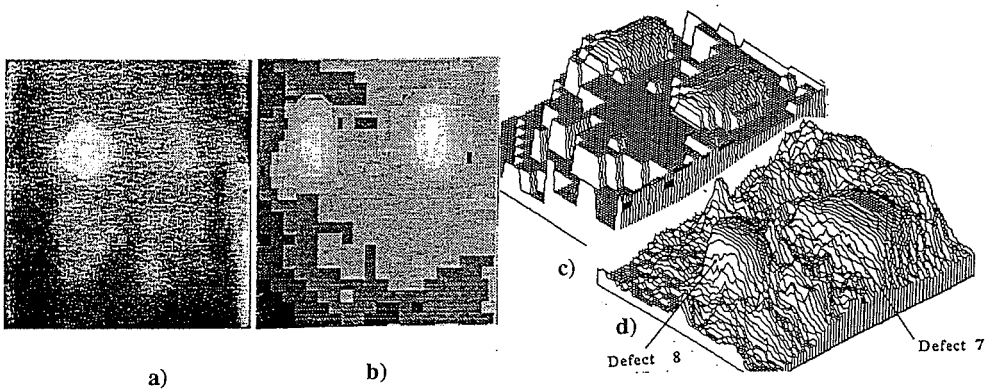

Fig. 3. - Examples of initial images: a) specimen 1, τ = 12 s, not filtered; b) specimen 2, τ = 12 s, filtered; c) 3D image of b); d) 3D image of specimen 2 tested from the opposite surface

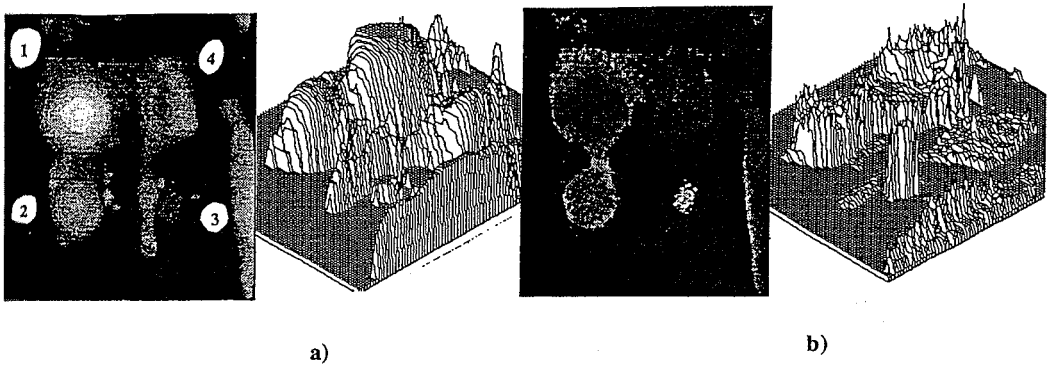

Fig. 4. - Examples of synthesized images for specimen 1: a) ΔT_m image; b) τ_m image

http://dx.doi.org/10.21611/qirt.1992.040

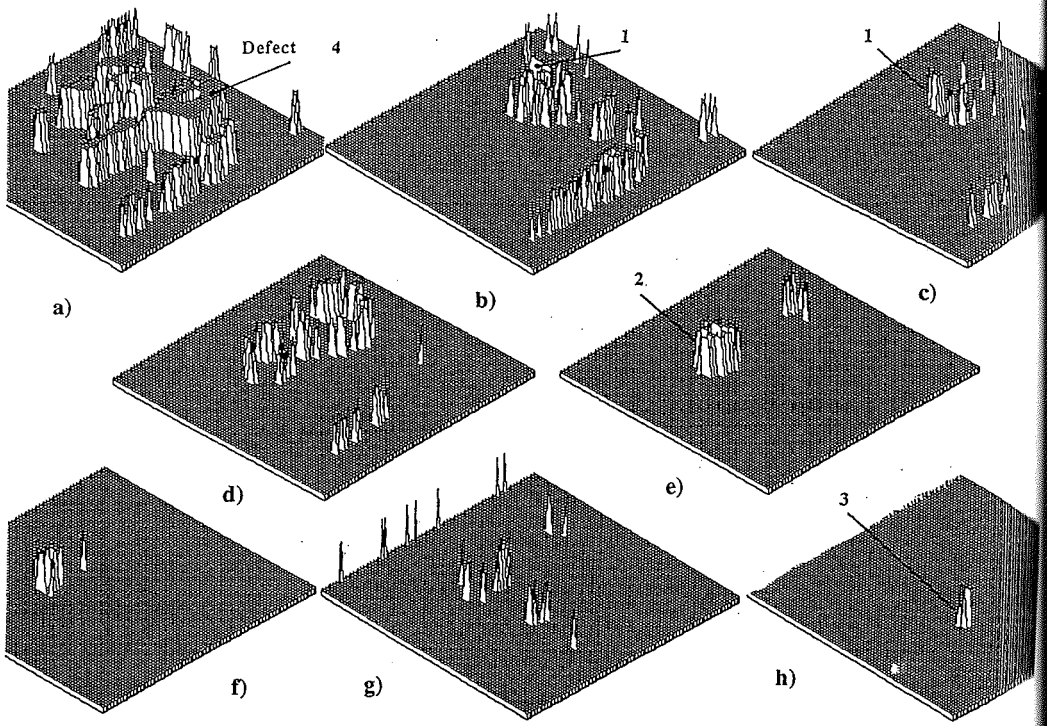

Fig. 5. - Tomograms of specimen 1: a) delay time range 0-6 s; b) 6-12 s; c) 12-18 s; d) 18-24 s; e) 24-30 s; f) 30-36 s; g) 36-48 s; h) 48-60 s

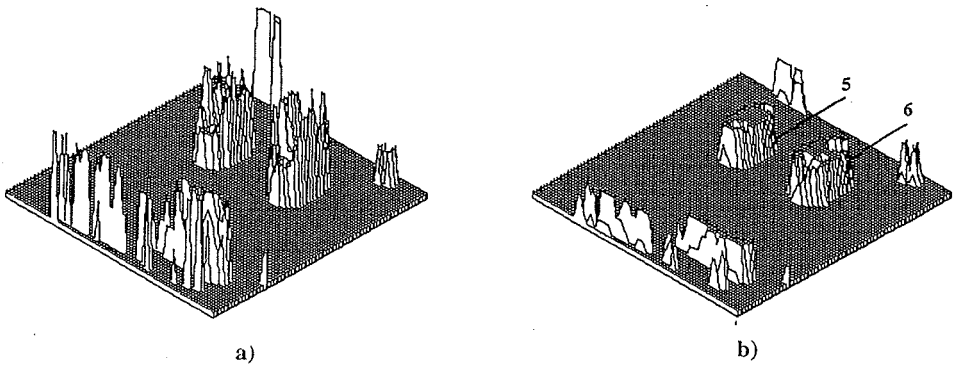

Fig. 6. - Tomograms of specimen 2 (delay time interval 7-35 s). a) normal (timegram); b) binary (tomogram)

http://dx.doi.org/10.21611/qirt.1992.040

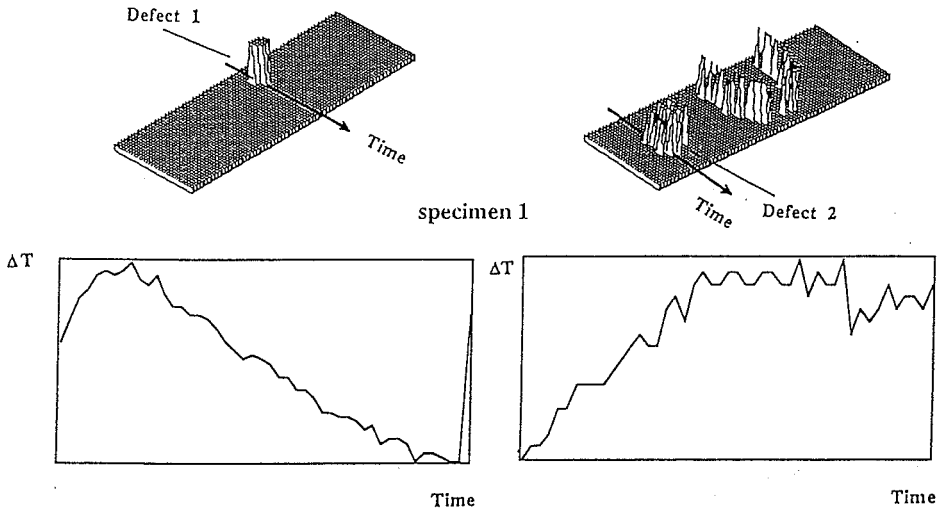

Fig. 7. - Cross-sectional timegrams of specimen 1 (profile across defects 1 and 2); stretching and slicing are used

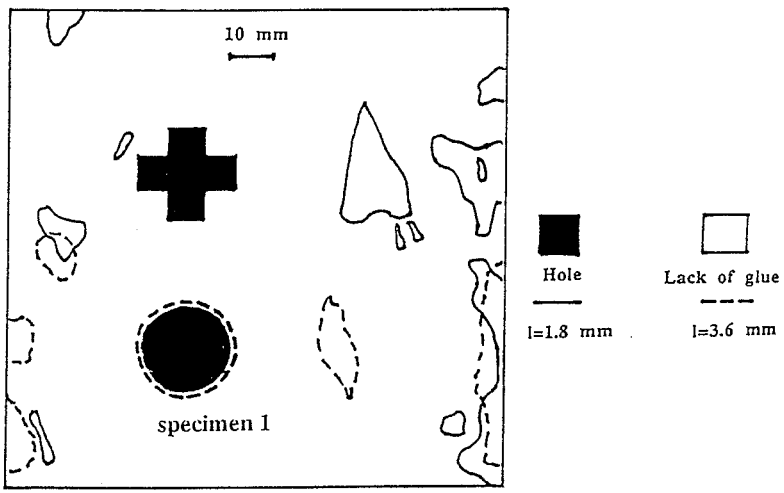

Fig. 8. - Superimposed scheme of artificial and real defects for two glued layers